19.5 Dual-Doppler Analyses of Nontornadic Supercells Observed with Mobile Ground-Based Doppler Radars

MARIO MAJCEN*, PAUL MARKOWSKI, AND YVETTE RICHARDSON
Department of Meteorology, Pennsylvania State University, University Park, PA

JOSHUA WURMAN
Center for Severe Weather Research, Boulder, CO

1. Introduction

Ever since the Verification of the Origins of Rotation in Tornadoes Experiment (VORTEX) the leading motivation for the collection of field observations in and near supercell thunderstorms was to improve our ability to discriminate between tornadic and nontornadic supercells. The low-level mesocyclone regions of supercells are routinely sampled by mobile Doppler radars at close range, with spatial resolution of less than 1 km, and temporal resolution on the order of 1–2 minutes or less. High resolution dual-Doppler observations (Beck et al. 2006; Wurman et al. 2007a,b) allow for three-dimensional analyses of kinematic fields that are superior to those available from the fixed Doppler radar networks relied upon in the past (e.g., Ray et al. 1975; Brandes 1977, 1981). Such observations can be used for detailed investigation of the mechanisms by which near-ground vertical vorticity maxima develop in supercell thunderstorms and the mechanisms that preclude additional amplification of vertical vorticity into a tornado. By analyzing a large number of storms it may be possible to identify recurring differences between tornadic and nontornadic supercells.

The purpose of this paper is to present dual-Doppler observations of two nontornadic supercells sampled by a pair of Doppler on Wheels (DOW) radars (Wurman et al. 1997) on 12 June 2004 and 18 June 2004 during the Radar Observations of Tornadoes and Thunderstorms Experiment (ROTATE). Our preliminary analysis is focused on low-level kinematic fields and on the rear-flank gust front structure.

An overview of the data set and analysis methods is given in section 2. Results are presented in section 3. Section 4 describes the tasks we will be undertaking in the upcoming months.

2. Data and methodology

The data set available for this study consists of dual-Doppler observations of four supercell thunderstorms sampled by a pair of DOW radars. The DOW radars are pulsed, pencil-beam, Doppler radars mounted on trucks. The wavelength and the stationary, half-power beamwidth of DOW radars are 3 cm and 0.93°, respectively. Only two of the observed supercells exhibited the low-level circulation similar to the low-level circulation found in tornadic supercells. Our study focuses on these two supercells: 12 June 2004 and 17 June 2004. In the latter case, the radar deployment started on 17 June 2004, but the dual-Doppler observations presented here are actually taken from 0025 UTC through 0030 UTC on 18 June 2004.

In the 12 June 2004 case, the DOW radars were deployed along a north-south line, east of the mesocyclone center with a baseline of 8.4 km. In the 18 June 2004 case, the DOW radars were deployed along a north-south line, but to the west of the mesocyclone center with a baseline of 10.6 km. The objectively analyzed three-dimensional winds were trusted only if the interbeam angle was between 30° and 150°.

The DOW data were rotated from a truck-relative reference frame to the earth-relative reference frame by aligning ground clutter targets with known locations of cell towers and the local road network. Ground clutter and other erroneous data were removed from the data set. After editing, the data were interpolated to a Cartesian grid using a 2-pass Barnes objective analysis technique (Barnes 1964; Majcen et al. 2008). In the 12 June 2004 case the grid dimensions are 17×17×3 km; in the 18 June 2004 case the grid dimensions are 21.2×21.1×3 km. The horizontal and the vertical grid spacing in both cases are 100 m.

Radar data are commonly interpolated to a Cartesian grid via an objective analysis. Most objective analysis methods allow one to filter scales that are poorly resolved in radar observations (Trapp and Doswell 2000) through judiciously chosen tuning parameters (e.g., smoothing parameter κ_0, and convergence parameter γ which typically are based on the data spacing, Δ). Multiple passes (i.e., successive corrections) of an objective analysis steepen the response function of the filter so that there is less damping at well-resolved scales (e.g., 8–20Δ) while still removing scales that are poorly resolved (e.g., $< 4\Delta$), (Koch et al. 1983). The resulting multi-pass objective analysis can provide a better fit to the observations than a single-pass objective analysis, while still suppressing the small-scale noise. In the 12 June 2004 case the smoothing parameter is $\kappa_0 = 0.15$ km^2; In the 18 June 2004 case the smoothing parameter is $\kappa_0 = 0.24$ km^2. In both cases convergence parameter is $\gamma = 0.3$.

3. Observations

Both supercells have circulation extending all the way to the lowest analysis levels (Fig. 1), and exhibit a structure simi-

*Corresponding author address: Mario Majcen, Department of Meteorology, Pennsylvania State University, 503 Walker Building, University Park, PA 16802; *e-mail*: mzm188@psu.edu

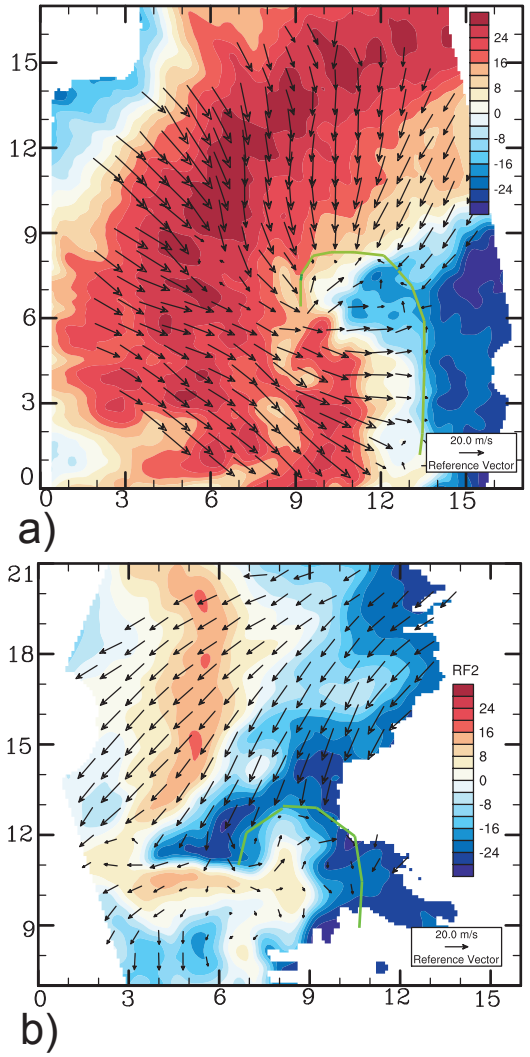

FIG. 1. (a) Horizontal cross-section of uncalibrated equivalent radar reflectivity factor (color shaded; see legend), and storm-relative wind vectors at 300 m AGL for the 2219 UTC wind synthesis on 12 June 2004. (b) As in (a), but for the 0025 UTC wind synthesis on 12 June 2004. Gust front location (green) is drawn for orientation purposes.

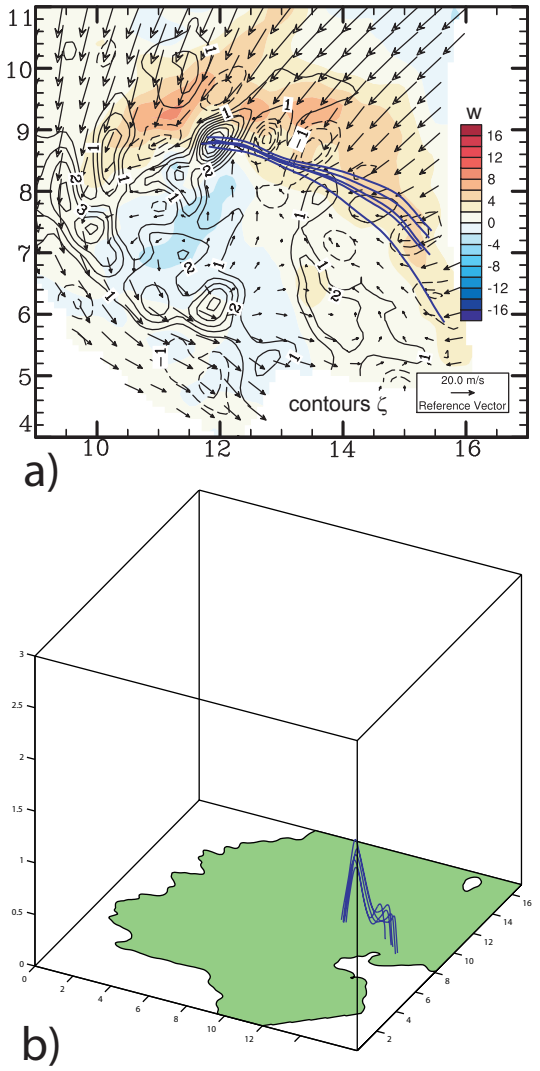

FIG. 2. (a) Horizontal cross-section of vertical velocity (color shaded; see legend), vertical vorticity (0.01 s^{-1} contours, dashed contours denote negative values, 0 s^{-1} contour suppressed for clarity) and storm-relative wind vectors at 300 m AGL for the 2219 UTC wind synthesis on 12 June 2004. Blue lines denote vortex lines projected onto 300 m AGL horizontal cross section. (b) Vortex lines originating from one of the vorticity maxima located along the gust front at 300 m AGL.

lar to the structure of low-level wind fields within tornadic supercells (e.g., Brandes 1977, 1978; Ray et al. 1981). The updrafts of both storms have a characteristic horseshoe appearance (Figs. 2a, and 3a). High resolution analyses of the gust front structure reveal multiple vertical vorticity maxima (Figs. 2a, and 3a) located along and near the respective gust fronts. The values of vertical vorticity associated with misocyclones located along the gust front are comparable or even larger than in some tornadic storms (e.g., Wurman et al. 2007b). However, the vorticity maxima associated with mesocyclones are weaker than in tornadic storms. The updraft at most analyses times does not extend to the mesocyclone region (e.g., Fig. 2a: $x = 11.5$ km, $y = 7$ km) so the near-ground mesocyclone is located in or near the rear-flank downdraft. At 0025 UTC 18 June there is a notable region of anticyclonic vorticity to the east of a weak mesocyclone (Fig. 3a).

Figure 4 depicts tilting and stretching terms of vertical vorticity equation at 2219 UTC 12 June 2004 and at 0025 UTC 18 June 2004 at 400 m AGL. Production of vertical vorticity by tilting is strongest along the gust front, on its northern side. Tilting is negative along the gust front on the rear-flank side of the gust front. In the mesocyclone regions of both storms the stretching is slightly negative which may explain relatively weak near-ground mesocyclone rotation.

2214 UTC 12 June 2004 is the only analysis time when the vertical vorticity associated with the near-ground mesocyclone (Fig. 5a: $x = 9.25$ km, $y = 7$ km) is considerably stronger than the vertical vorticity associated with the gust front misocyclones (Fig. 5a: $x = 10.25$ km, $y = 7.5$ km). The mesocyclone is located in the updraft, and the rear-flank downdraft

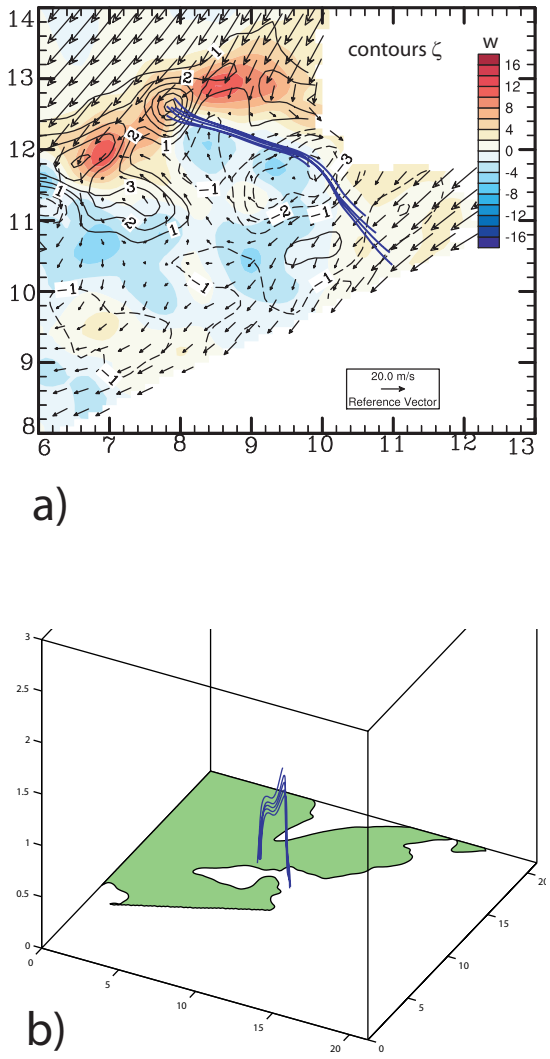

FIG. 3. As in Fig. 2 but at 300 m AGL for the 0025 UTC wind synthesis on 18 June 2004.

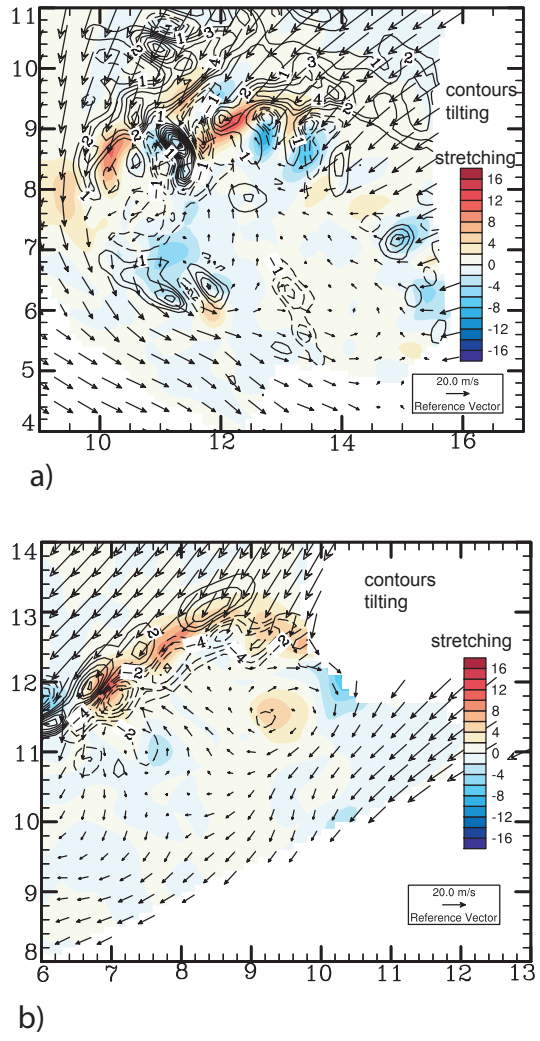

FIG. 4. (a) Horizontal cross-section of stretching (color shaded; see legend), tilting ($2\times$ 10^{-4} s^{-2} contours, dashed contours denote negative values, 0 s^{-2} contour suppressed for clarity) and storm-relative wind vectors at 400 m AGL for the 2219 UTC wind synthesis on 12 June 2004. (b) As in (a) but for 0025 UTC 18 June 2004.

is slightly stronger than at other analysis times. The vorticity maximum associated with the mesocyclone is located in a small region of very strong stretching (Fig. 5b).

Some vortex lines originating in those vorticity maxima form arches that connect the vertical vorticity maxima with regions of negative vertical vorticity found farther south along the gust front (Fig. 2b, and Fig. 3b). In both the 12 June , and the 18 June case, the vortex line arches projected onto a horizontal cross section of the low-level wind field (Fig. 2a, and Fig. 3a) show that the arches are approximately parallel to the low-level gust front. Other vortex lines originating in the vorticity maxima located near or along the main updraft extend almost vertically (not shown) to the highest data level (usually around 2 km AGL in the main updraft region) so it cannot be inferred whether they also form arches or not. This is especially true for the vorticity maxima found farther away (to the south, or southwest) from the main updraft.

At all analyses times the strong low-level horizontal vorticity is observed along the gust front (Fig. 6) and the orientation of the horizontal vorticity vectors indicates strong baroclinic vorticity generation.

4. Summary and future work

Both nontornadic supercells analyzed in this study have a kinematic structure very similar to the tornadic supercells: (1) gust front structure is occluded, (2) the updraft has a characteristic horseshoe-shaped appearance, (3) multiple misocyclones can be found along the gust front.

A prominent difference between both nontornadic supercells analyzed in this study and tornadic supercells is the location of the near-ground mesocyclone with respect to the updraft. At all except one analysis time, the near-ground mesocyclone is not located in the updraft. At the analysis time when the mesocyclone is located in the near-ground updraft it is much stronger

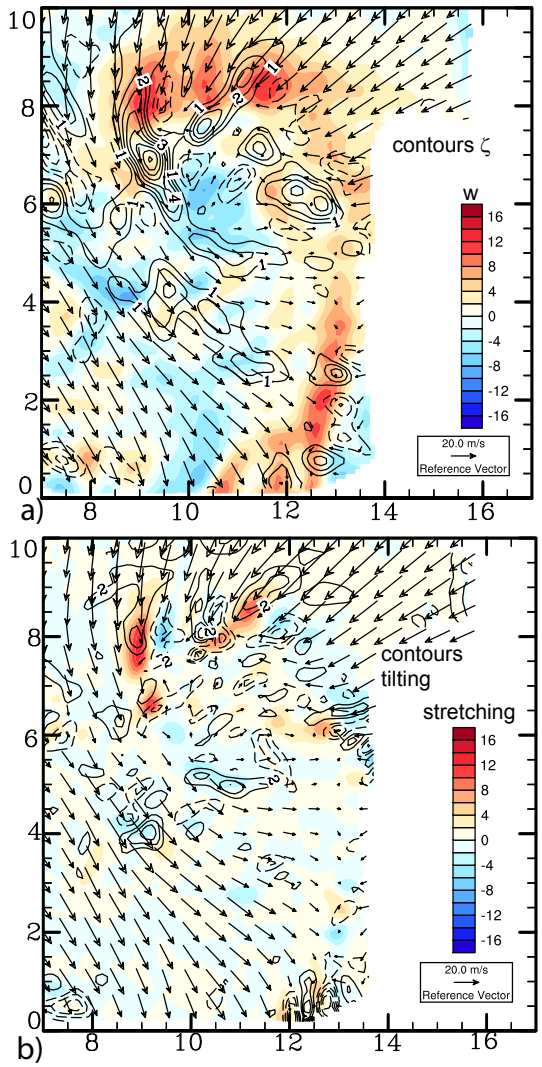

FIG. 5. (a) Horizontal cross-section of vertical velocity (color shaded; see legend), vertical vorticity (0.01 s^{-1} contours, dashed contours denote negative values, 0 s^{-1} contour suppressed for clarity) and storm-relative wind vectors at 300 m AGL for the 2214 UTC wind synthesis on 12 June 2004. (b) Horizontal cross-section of stretching (color shaded; see legend), tilting (10^{-4} s^{-2} contours, dashed contours denote negative values, 0 s^{-2} contour suppressed for clarity) and storm-relative wind vectors at 300 m AGL for the 2214 UTC wind synthesis on 12 June 2004.

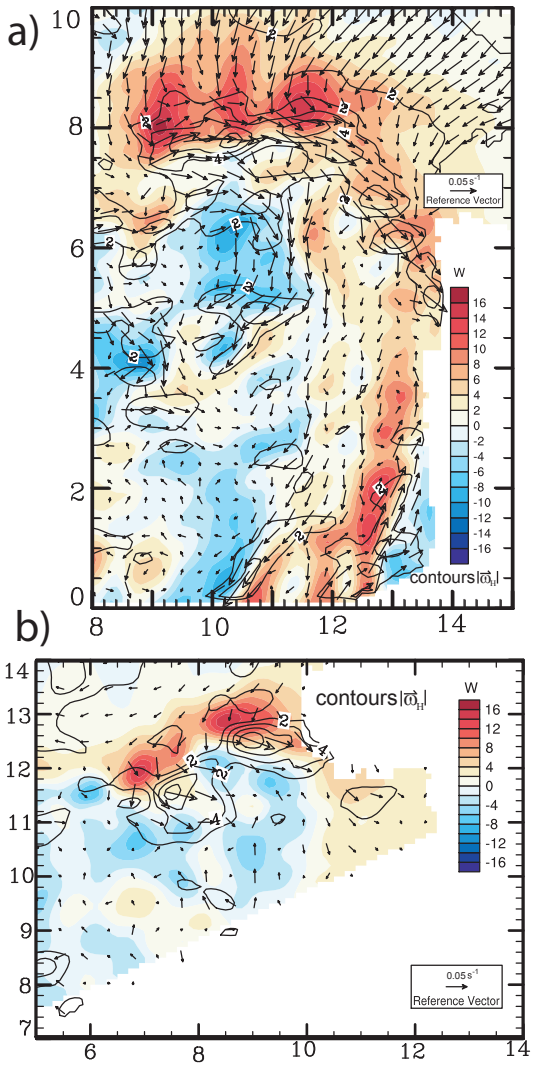

FIG. 6. (a) Horizontal cross-section of vertical velocity (color shaded; see legend), horizontal vorticity (0.02 s^{-1} contours, dashed contours denote negative values, 0 s^{-1} contour suppressed for clarity) and horizontal vorticity vectors at 400 m AGL for the 2214 UTC wind synthesis on 12 June 2004. (b) As in (a) but for the 0025 UTC wind synthesis on 18 June 2004.

than at other analysis times due to strong stretching of vertical vorticity.

Arching of vortex lines and the orientation of horizontal vorticity vectors along the gust front suggest that tilting of baroclinically generated horizontal vorticity into vertical vorticity may be an important mechanism for generating vertical vorticity in the gust front region of nontornadic supercells. Strong baroclinic vorticity generation along the rear-flank gust front can be indicative of an excessively cool downdraft air. This is consistent with very weak or nonexistent near-ground updraft in the mesocyclone region. Previous studies (e.g., Markowski et al 2002) have shown that excessively cool downdrafts are detrimental to tornadogenesis.

In the upcoming months, we hope to analyze more nontornadic storms and compare our observations to tornadic supercells. Some of the questions we hope to answer are: Given the lack of direct thermodynamical observations in the low levels of both tornadic and nontornadic supercells and assuming that the horizontal vorticity along the gust front is mostly due to baroclinic generation there: can the strength of horizontal vorticity along the gust front be used as a proxy for estimating buoyancy deficits of the downdraft air? In our observations, the rear-flank gust front and the updraft rarely extend all the way to the near-ground mesocyclone. How does this compare to the near-ground mesocyclones in tornadic storms? Some previous studies have documented the double gust front structure in tornadic supercells, can similar structures be found in nontornadic storms?

Acknowledgments. We wish to thank Ryan Hastings, Kent Knopfmeier, James Marquis, and Jeffrey Frame on their suggestions and inspiring discussions, as well as numerous ROTATE participants (too many to mention). Support from NSF grant ATM-0437512 and ATM-0437505 is also acknowledged.

REFERENCES

Barnes, S. L., 1964: A technique for maximizing details in numerical weather map analysis. *J. Appl. Meteor.*, **3**, 396–409.

Beck, J. R., J. L. Schroeder, and J. M. Wurman, 2006: High-resolution dual-Doppler analyses of the 29 May 2001 Kress, Texas, cyclic supercell. *Mon. Wea. Rev.*, **134**, 3125–3148.

Brandes, E. A., 1977: Flow in a severe thunderstorm observed by dual-Doppler radar. *Mon. Wea. Rev.*, **105**, 113–120.

Brandes, E. A., 1978: Mesocyclone evolution and tornadogenesis: Some observations. *Mon. Wea. Rev.*, **106**, 995–1011.

Brandes, E. A., 1981: Finestructure of the Del City-Edmond tornadic mesocirculation. *Mon. Wea. Rev.*, **109**, 635–647.

Koch, S. E., M. desJardins, and P. J. Kocin, 1983: An interactive Barnes objective map analysis scheme for use with satellite and convetional data. *J. Atmos. Sci.*, **22**, 1487–1503.

Majcen, M., P. Markowski, Y. Richardson, D. Dowell and J. Wurman, 2007: Multi-pass objective analyses of Doppler radar data. *J. Atmos. Oceanic Technol.*, **25**, 1845-1858.

Markowski, P. M., J. M., Straka and E. N. Rasmussen, 2002: Direct surface thermodynamic observations within the rear-flank downdrafts of nontornadic and tornadic supercells. *Mon. Wea. Rev.*, **130**, 1692–1721.

Markowski, P., E. Rasmussen, J. Straka, R. Davies-Jones, Y. Richardson, and R.J. Trapp, 2008: Vortex lines within low-Level mesocyclones obtained from pseudo-dual-Doppler radar observations. *Mon. Wea. Rev.*, **136**, 3513–3535.

Ray, P. S., R. J. Doviak, G. B. Walker, D. Sirmans, J. Carter, and B. Bumgarner, 1975: Dual-Doppler observation of a tornadic storm. *J. Appl. Meteor.*, **14**, 1521–1530.

Ray, P. S., J. B. Klemp, R. B. Wilhemson, 1981: Observed and numerically simulated structure of a mature supercell thunderstorm. *J. Atmos. Sci.*, **38**, 1558–1580.

Trapp, R. J., and C. A. Doswell III, 2000: Radar data objective analysis. *J. Atmos. Oceanic Technol.*, **17**, 105–120.

Wurman, J. M., J. M. Straka, E. N. Rasmussen, M. Randall, and A. Zahrai, 1997: Design and deployment of a portable, pencil-beam, pulsed, 3-cm Doppler radar. *J. Atmos. Oceanic Technol.*, **14**, 1502–1512.

Wurman, J., Y. Richardson, C. Alexander, S. Weygandt, and P. F. Zhang, 2007a: Dual-Doppler and single-Doppler analysis of a tornadic storm undergoing mergers and repeated tornadogenesis. *Mon. Wea. Rev.*, **135**, 736–758.

Wurman J., Y. Richardson, C. Alexander, S. Weygandt, and P. F. Zhang, 2007b: Dual-Doppler analysis of winds and vorticity budget terms near a tornado. *Mon. Wea. Rev.*, **135**, 2392–2405.